Batteries & Supercaps

Research Article
doi.org/10.1002/batt.202400744

Chemistry Europe
European Chemical Societies Publishing

www.batteries-supercaps.org

Glyme-based Localized High Concentration Electrolytes Improve the Stability of Na-ion Battery Materials in Half-cells

Meena Ghosh,*[a, c] Neelam Yadav,[a] and Philipp Adelhelm*[a, b]

Sodium-ion batteries (SIBs) have emerged as promising alternatives to lithium-ion batteries for grid energy storage and automotive applications. However, their widespread adoption necessitates improved cycling stability and energy density, largely dependent on electrode materials and electrolytes. This study investigates the compatibility and performance of the diglyme-based localized high concentration electrolyte (LHCE/G2) for SIB applications, proposing it as the electrolyte of choice for materials screening in half-cell configuration. Three layered oxide cathode materials were tested in LHCE/G2 against sodium metal counter electrodes, demonstrating significantly enhanced cycling stability compared to carbonate electrolytes. The electrochemical stability of LHCE/G2 on sodium metal was confirmed through long-term plating/stripping profiles. The findings suggest that glyme-based LHCEs offer a promising approach to evaluating high-voltage oxide cathodes, minimizing electrolyte-related degradation, and enhancing the reliability and performance of SIBs.

Introduction

Sodium-ion batteries (SIBs) have demonstrated practical viability as an alternative to lithium-ion batteries in grid energy storage and automotive applications. However, their widespread implementation and intrusion into commercial applications demand improved cycling stability and energy density. These aspects depend on various factors, including the choice of electrode materials and electrolytes in SIB cells. Therefore, research in this field is focused on developing new materials to unlock the full potential of SIB technology. Among the large variety of cathode materials identified to date, electrode materials, such as layered transition metal oxides (LMOs) stand out by offering high operating voltage, high specific capacity, and scope to leverage the established manufacturing processes from lithium-ion batteries (LIBs).[1] However, the complex electrochemical reactions and phase transitions of high-voltage cathodes cause performance degradation over cycling. There have been attempts to stabilize cathodes at the material level by morphology tuning, surface coating, doping, etc.[2] However, the lack of electrolytes stable at higher voltage imparts challenges concerning the intrinsic electrochemical characterization of these cathode materials[3] – therefore, suppressing the negative impact of an otherwise unstable electrolyte on the overall performance is essential.

Similar to cathodes, unstable electrolytes also impart intricacies to the lab-scale evaluation of the key performance parameters of a new electrode material in a half-cell configuration consisting of Na metal counter electrode.[4] The limitation is pronounced in conventional liquid electrolytes containing carbonate solvents. The high reactivity of Na metal and low reduction stability of carbonate solvents result in electrolyte decomposition, leading to unfavourable electrochemical properties.[5] Electrolytes consisting of different additives, or a mixture of various carbonate solvents are proposed to improve the compatibility of sodium metal anode and electrolyte.[6] However, no standard composition has been identified that can simultaneously address the issues related to the metal anode and high-voltage cathodes, and multiple components in the electrolyte increase complexity and add ambiguity when attempting to make conclusions regarding failure mode and root cause analysis.

To address the limitations imposed by the electrolyte on cell performance during materials evaluation, it's crucial to develop an electrolyte specifically tailored to be compatible with both, the metal anode and high-voltage cathodes. Unlike carbonate electrolytes, ether-based electrolytes are more stable against Na metal and are proposed to be an alternative to carbonate counterparts. For instance, the compatibility of diglyme-based electrolytes against Na has been discussed in several reports.[7] From first principle calculations, Xu et al.,

[a] Dr. M. Ghosh, Dr. N. Yadav, Prof. Dr. P. Adelhelm
Institut für Chemie
Humboldt Universität zu Berlin
Brook-Taylor-Str.2, 12489 Berlin, Germany
E-mail: meena.ghosh@hu-berlin.de
philipp.adelhelm@hu-berlin.de

[b] Prof. Dr. P. Adelhelm
Joint Research Group Operando Battery Analysis
Helmholtz-Zentrum Berlin
Hahn-Meitner-Platz1, 14109 Berlin, Germany

[c] Dr. M. Ghosh
Holst Center
TNO
5656 AE, The Netherlands
E-mail: meena.ghosh@tno.nl

Supporting information for this article is available on the WWW under https://doi.org/10.1002/batt.202400744

concluded that the energy level of the lowest unoccupied molecular orbital (LUMO) of mono- and diglyme lies above the LUMO level of the carbonate esters (ethylene carbonate (EC), propylene carbonate (PC), etc.).[8] Therefore, glymes show better reductive stability and undergo less electrochemical degradation on the Na counter electrode than carbonates. However, their lower oxidation stability due to the high energy highest occupied molecular orbital (HOMO) makes glymes less suited with cathodes that operate at relatively high voltage. In addition, the stability of a Na metal electrode is also highly dependent on the conductive salt used, with NaTFSI causing rapid Na metal corrosion.[7b] As a result, carbonate electrolytes, typically containing $NaPF_6$ as conductive salt, remained the most viable option for SIB evaluation.

A straightforward way to improve the anodic (= high voltage) stability of glymes is minimizing the number of free-solvent molecules in the electrolyte by using very high salt concentration (3-5 M), thereby conceiving high concentration electrolytes (HCEs).[9] Nevertheless, the HCE concept involves a notable trade-off in terms of ionic conductivity and viscosity when compared to standard concentration (1 M) electrolytes. Conversely, glyme-based localized high concentration electrolytes (LHCEs), which introduce an inert miscible solvent with a low dielectric constant as a diluent to HCE, have proven to be an effective approach. Due to its non-polar nature, the second solvent or diluent doesn't disrupt the solvation shell of the primary solvent, thereby retaining the highly concentrated salt-solvent cluster in the local environment while adjusting the concentration of the whole electrolyte mixture to a dilute state.[10] As a result, LHCEs combine the traits of HCEs in terms of high oxidative stability while showcasing comparable viscosity and ionic conductivity as of the standard electrolytes.[11] Recent studies also indicate that LHCE promotes the formation of a salt-derived solid electrolyte interphase rich in inorganic components.[12] However, it must be noted that the choice of non-polar diluents (typically hydrofluoroethers) in the LHCE composition can also impact the nature of the interphase.[13]

This work investigates the compatibility of diglyme-based LHCE (LHCE/G2) for sodium-ion battery research and recommends as the preferred electrolyte for materials screening in half-cell configuration. As a proof-of-concept, three different LMO cathodes (P2-$Na_{2/3}Fe_{1/2}Mn_{1/2}O_2$, P2-$Na_{2/3}Ni_{1/3}Mn_{2/3}O_2$, and O3-$NaNi_{1/3}Fe_{1/3}Mn_{1/3}O_2$) with high operating voltage were tested in LHCE/G2 against Na metal counter electrode, and the electrochemical performance was evaluated. The results show that LHCE/G2 enabled significantly better cycling stability of the LMOs compared to dilute carbonate electrolytes. For example, the cycling stability of P2-$Na_{2/3}Fe_{1/2}Mn_{1/2}O_2$ cathode in LHCE/G2 showed 65% retention of initial capacity after 150 cycles whereas the same in $NaPF_6$/PC was found to be only 35%. The compatibility of LHCE to Na metal was evident from the long-term plating/stripping profile of the Na|Na symmetric cells. The electrochemical stability of LHCE/G2 was better than the dilute carbonate counterpart based on the current-voltage profile in the linear sweep voltammetry (LSV) curve. The findings of this study underline that LHCEs, for their Na metal compatibility and high voltage stability, are suitable choices to evaluate SIB materials in half-cell configuration. More investigation in this direction would be interesting for sodium batteries inspired by the success of this new electrolyte chemistry (LHCE) in lithium batteries.

Results and Discussion

In this study, diglyme (G2) was used as the base solvent for LHCE preparation along with NaFSI as the Na salt and 1, 1, 2, 2-tetrafluoroethyl-2, 2, 3, 3-tetrafluoropropyl ether (TTE) as the diluent. The G2-based dilute electrolyte was prepared using a 1 M concentration of NaFSI in G2 solvent (DE/G2) for comparison. Like LHCE/G2, two other linear ether solvents with different chain lengths, dimethyl ether (G1) and triglyme (G3), were also considered as the solvating solvents for the LHCEs. To optimize the electrolyte oxidation stability, LHCEs were prepared by adjusting the salt/ether molar ratios to near saturation levels. The resulting LHCE formulations include LHCE/G1 (1.0NaFSI-2.25G1-3.0TTE), LHCE/G2(1.0NaFSI-1.5G2-3.0TTE), and LHCE/G3 (1.0NaFSI-1.12G3-3.0TTE). All three LHCEs contained the same mole ratio of Na^+ and ether O from the solvating solvent glyme ($[Na^+]/[O] = 1/4.5$).

The Fourier-transform infrared spectroscopy (FTIR) data of the NaFSI salt, neat G2 and TTE solvents, and electrolyte mixtures are compared in Figure S1. A shift of a few characteristic peaks of neat G2 (e.g., at 1101, 1026, and 852 cm^{-1}) and the appearance of new peaks (at 1081 cm^{-1}) are observed in the DE/G2, HCE/G2, and LHCE/G2, indicating ion-solvent interaction in different electrolytes. In addition, the FTIR peak of neat G2 at 1199 cm^{-1} is absent in HCE/G2 and LHCE/G2, which also gives a good indication regarding the interactions between the oxygen group of ether and Na^+ ion.

For a better understanding of the evolution of the solvation structures, the salt, solvent, and electrolytes were further characterized by Raman spectroscopy (Figure 1a and Figure S2). As displayed in Figure 1b, the characteristic ether peaks in neat G2 appear in the frequency range of 760–900 cm^{-1}. The peaks at 804, 827, and 850 cm^{-1} observed in neat G2 are also present in the DE/G2 due to the abundant amount of free G2 molecules in the dilute electrolyte. Besides, the DE/G2 shows two new peaks at 842 and 869 cm^{-1} assigned to the ether moieties bound to the Na^+ ions. These peaks appear pronounced at a high salt concentration (HCE/G2) while the peaks related to free G2 becomes less prominent. As a result, the characteristic ether peaks of neat G2 are found to disappear in the HCE/G2 verifying that the concentrated electrolyte contains hardly any free ether groups.

Variations in salt-solvent interactions, influenced by electrolyte concentration, are evident from the Raman peaks corresponding to the FSI^- anion (Figure 1c). Specifically, the FSI^- peak in DE/G2 (718 cm^{-1}) demonstrates a red shift in comparison to pure NaFSI salt (753 cm^{-1}), indicating weaker coordination between Na^+ and FSI^- ions in the dilute electrolyte due to robust ion solvation. The position of the FSI^- peak in the HCE/G2 at 734 cm^{-1} appears between DE/G2 and pure NaFSI. This

Research Article
doi.org/10.1002/batt.202400744
Chemistry Europe
European Chemical Societies Publishing

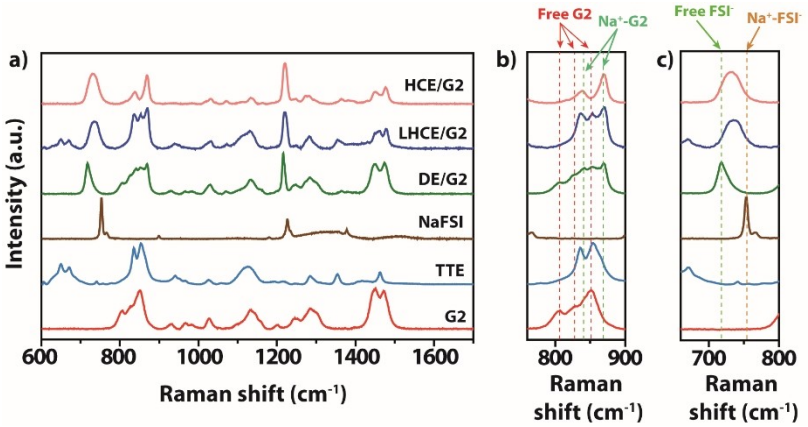

Figure 1. (a) Raman spectra of G2, TTE, NaFSI, and various electrolytes (HCE/G2, LHCE/G2, DE/G2); Raman spectra indicating the shift in characteristic peaks of (b) ether group (between 750–900 cm^{-1}) and (c) FSI^- moiety (between 650–800 cm^{-1}) in different electrolytes. (G2 – diglyme, TTE - tetrafluoroethyl tetrafluoropropyl ether, DE – dilute electrolyte, HCE – high concentration electrolyte, LHCE – localized high concentration electrolyte).

trend illustrates the stronger coordination between Na^+ and FSI^- ions in HCE/G2 compared to that in DE/G2 due to the partial solvation of ions and the presence of contact ion pairs in concentrated electrolyte solutions.

Interestingly, the dilution of HCE/G2 with TTE solvent does not alter the location and overall shape of the characteristic peaks for both the ether group and FSI^- anion in LHCE/G2. This is because of the nonpolar nature of TTE that doesn't interrupt the solvation structures formed in the concentrated electrolyte. Therefore, TTE remains an inert component in the electrolyte system. It can also be noted that the ether peaks of TTE molecules in LHCE overlap with that of neat TTE which further supports no or negligible association of TTE in the ion solvation chemistry. Besides, the other LHCEs prepared with G1 (Figure S3a) and G3 (Figure S3b) as the base solvents also show similar interactions in the Raman. These results signify that the diluent properties of TTE hold true in Na^+-salt-based LHCEs as reported for the Li counterpart.

Concentrated electrolytes, while offering various advantages, are hindered by their diminished ionic conductivity compared to the conventionally employed dilute electrolytes. Illustrated in Figure 2a, the DE/G2 exhibits higher conductivity (9.3 mS cm^{-1} at 20 °C) over HCE/G2 (2.3 mS cm^{-1} at 20 °C) across a broad temperature range. Notably, HCE/G2 demonstrates a pronounced deviation from the linear correlation between conductivity and temperature, particularly in the lower temper-

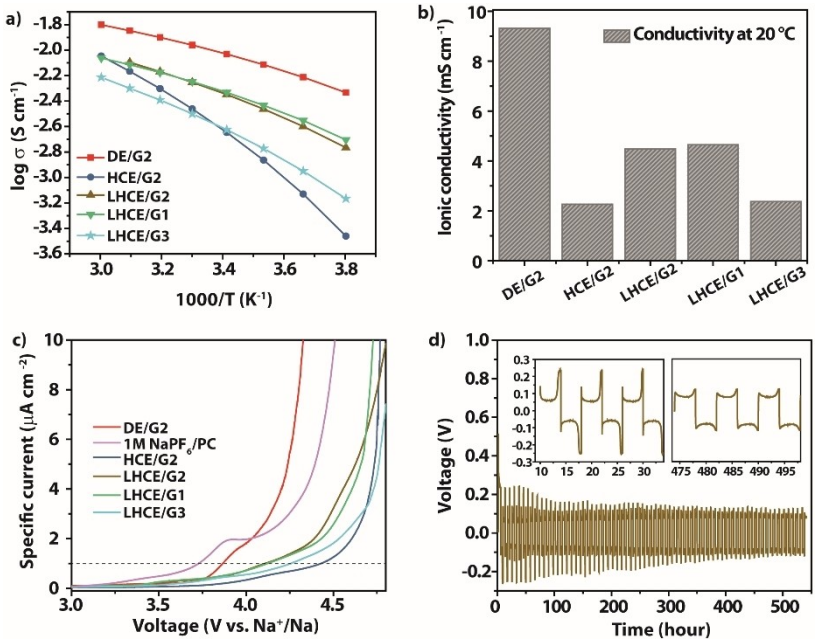

Figure 2. (a) Temperature dependence of ionic conductivity, (b) ionic conductivity at 20 °C, (c) anodic stability window for DE/G2, 1 M $NaPF_6$/PC, HCE/G2, and LHCEs; (d) voltage vs. time profile for sodium plating/stripping in LHCE/G2 electrolyte at 0.12 mA cm^{-2} current density. (G1 – monoglyme, G2 – diglyme, G3 – triglyme, PC – propylene carbonate, DE – dilute electrolyte, HCE – high concentration electrolyte, LHCE – localized high concentration electrolyte).

ature range. The conductivity of LHCE/G2 (4.5 mS cm^{-1} at 20 °C) falls between these extremes, indicating enhanced ion mobility due to reduced viscosity from the addition of TTE, as opposed to HCE/G2. However, the presence of ion-pair aggregates in LHCE results in a diminished number of ionic species available for conduction. Furthermore, the sluggish mobility of charged ion-pair aggregates impairs the overall ion transport properties of the electrolyte.[14] The combined impact of these factors accounts for the comparatively lower conductivity of LHCE/G2 in contrast to DE/G2. Figure 2a and b also illustrate comparable conductivities between LHCE/G1 and LHCE/G2, while LHCE/G3 displays a lower conductivity due to the high viscosity of the G3 solvent. Moreover, the conductivity of LHCE/G2 and LHCE/G1 appears higher or comparable to many of the commonly used ionic-liquid-based electrolytes explored earlier in SIBs.[15] It is noted that the conductivity of the glyme-based concentrated electrolytes is less than the dilute electrolytes of carbonate solvents (e.g., 0.5 M $NaPF_6$/PC) displaying ionic conductivity of 5.4 mS cm^{-1} at 20 °C, Figure S4). While low ionic conductivity can increase resistance in battery cells, particularly at very high C-rates, its impact at low currents typically used in lab-scale evaluation of new battery materials is minimal. Nevertheless, ionic conductivity alone does not determine the overall performance of an electrolyte; other properties, such as oxidation stability and compatibility with electrode materials, are equally important, as discussed later in this study.

The anodic stability of the electrolytes was assessed in a cell configuration with a Na metal counter electrode and carbon-coated Al (C/Al) working electrode using the Linear Sweep Voltammetry (LSV) technique at a scan rate of 0.1 mV sec^{-1}. As given in Figure 2c, the LSV curve of DE/G2 shows a significant increase in the current response from 3.7 V (vs. Na^+/Na) due to the electrochemical oxidation of the electrolyte components. On the other hand, the LSV profiles of HCE/G2 and LHCE/G2 tracing a negligible current density ($< 1\ \mu m\ cm^{-2}$) below 4.1 V vs. Na^+/Na indicate their improved oxidation stability compared to DE/G2. A similar LSV profile was also obtained for LHCE/G1 and LHCE/G3. Moreover, considering the onset voltage corresponding to the current density of 1 $\mu A\ cm^{-2}$ (indicated by the dashed line in Figure 2c), the anodic stability of all three LHCEs was better compared to 1 M $NaPF_6$/PC. Overall, the stability for the 1 $\mu A\ cm^{-2}$ limit decreases in the order: (most stable) HCE/G2 (4.4 V vs. Na^+/Na) > LHCE (4.2-4.1 V vs. Na^+/Na) > DE/G2 > 1M $NaPF_6$/PC (least stable). The low stability of dilute electrolytes can also be affected by the corrosive nature of NaFSI salt on the Al current collector, a phenomenon that is more pronounced in conventional carbonate-based electrolytes. Studies have shown that in carbonate-based dilute electrolytes, such as NaFSI/PC, oxidation begins at voltages above 3.6 V vs. Na^+/Na.[16] Such corrosion issue is already known to be alleviated by employing alternative electrolytes such as HCEs and LHCEs.[17] While the findings of this study highlight the advantage of LHCEs in terms of oxidation stability, they also emphasize the benefits of ether-based electrolytes over their commonly used carbonate counterparts.

It's important to acknowledge that the LSV technique, employed in this study for determining the electrochemical stability window of electrolytes, has limitations.[18] This is due to the use of an inactive working electrode, such as C/Al and the two-electrode geometry. In contrast, a real cell features a working electrode composed of active materials with redox-active metal centers such as Ni, Mn, or Fe. These metal centers can act as catalysts, accelerating electrolyte decomposition at high voltages. Furthermore, unlike non-active electrodes, real electrodes are porous and possess a higher surface area, which can further enhance electrolyte decomposition. Consequently, the oxidation stability of an electrolyte measured by LSV (using non-active materials) may differ slightly from that observed in real cells. Therefore, the measurements provide a relative comparison of electrolyte stability within the context of this study for preliminary screening and may not reflect their absolute stability limits. Nonetheless, the observed cycling stability of various cathode active materials (CAM) in these electrolytes, as discussed in subsequent sections, aligns well with the results obtained from the LSV studies.

The compatibility of the LHCEs with the Na electrode was studied in Na|Na symmetrical cells. The plating and stripping of Na was carried out at a constant current of 0.12 mA cm^{-2} with an areal capacity of 0.5 mAh cm^{-2}. The cell with LHCE/G2 exhibits (Figure 2d) a relatively high overpotential (0.45 V) in the initial few cycles followed by a stable cycling over 500 h with a reduction in the overpotential to 0.22 V. The voltage *vs.* time profile of the cell shows a noticeable change over cycling. In the inset of Figure 2d, the initial cycles show a sharp voltage spike/dip at the beginning and end of the plating and stripping processes. These features could be due to the nucleation overpotential and formation of electrolyte concentration gradient near the electrode surface.[19] However, the voltage profile features plateau-like characteristics without sharp voltage spike/dip as the cycles progressed, suggesting the formation of a stable interphase on the surface of Na metal over cycling. Moreover, the long-term cycling of the LHCE/G2 cell beyond 500 hrs. evidences the good compatibility of the electrolyte with Na metal. A similar plating/stripping feature was obtained in LHCE/G1 (Figure S5a) and LHCE/G3 (Figure S5b) electrolytes with overpotential values of 0.13 and 0.24 V, respectively.

On the other hand, the dilute carbonate electrolyte 1 M $NaPF_6$/PC initially showed lower polarization (0.2 V). However, a substantial increase in the polarization to ~0.4 V was observed over cycling (Figure S5c). This suggests that the interphase formed on the Na metal surface 1 M $NaPF_6$/PC during cycling led to increased resistance to sodium plating and stripping. This increase in resistance with cycling is often overlooked in a full cell. For instance, in the two-electrode coin cells often used for research purposes, the resistance developed on the Na metal counter electrode can lead to an underestimation of the stability of cathode active materials, as the cut-off voltage is reached earlier the longer the cell is cycled. These findings therefore highlight the limitations of dilute carbonate electrolytes for evaluating SIB materials in half-cell configurations with a Na metal electrode. It is important to mention that glyme-based dilute electrolytes containing $NaPF_6$ salt have also been investigated for their compatibility with Na metal anode.[7a]

Research Article
doi.org/10.1002/batt.202400744
Chemistry Europe
European Chemical Societies Publishing

Nevertheless, their high-voltage stability remains ambiguous due to the presence of uncoordinated solvent molecules.[20]

After the preliminary characterization, the merits of the LHCE/G2 electrolyte were further investigated in the half-cell configuration using three different high-voltage layered transition metal oxide cathode materials. The materials considered in this study belong to P2 and O3 phases with stoichiometries of $Na_{2/3}Fe_{1/2}Mn_{1/2}O_2$ (P2-FMO), $Na_{2/3}Ni_{1/3}Mn_{2/3}O_2$ (P2-NMO), and $NaNi_{1/3}Fe_{1/3}Mn_{1/3}O_2$ (O3-NFMO). While the electrochemical properties of these materials against Na counter electrode in carbonate electrolytes are well explored in the literature, they often suffer from poor cycling stability. This instability is attributed to phase changes and structural degradation of the materials triggered by their electrochemical reactions with Na^+ ions. For example, a detailed study on the degradation of P2-type material $Na_{2/3}Mn_{3/4}Ni_{1/4}O_2$ has been reported by Pfeiffer et al.[21] At the same time, it is worth noting that many of the currently commercialized SIBs contain NFMO as cathode active material. This suggests that the rising resistance of the Na counter electrode in carbonate electrolytes indeed leads to an underestimation of the cathode stability.

Figure 3a and b show the charge & discharge curves for the P2-FMO cathode in LHCE/G2 and 0.5 M $NaPF_6$/PC electrolytes, respectively. During charging, the two weak redox plateaus appeared close to 3.0 and 3.8 V *vs.* Na^+/Na in both cases, which are characteristics of P2-FMO. The cell with 0.5 M $NaPF_6$/PC shows an additional plateau above 4.0 V in the 1st cycle. The same plateau is observed in 2nd and following charge cycles in LHCE/G2. However, the voltage profiles (except for the 1st cycle) in 0.5 M $NaPF_6$/PC trace a higher charge capacity than in discharge, resulting in low Coulomb efficiency (Figure 3c). On the other hand, the charge and discharge curves of P2-FMO in LHCE/G2 trace equal capacity and better Coulomb efficiency compared to that in 0.5 M $NaPF_6$/PC. This difference indicates the possibility of irreversible electrolyte decomposition at the higher operating voltage in 0.5 M $NaPF_6$/PC, which is also evident from the LSV profile of the PC-based electrolyte in Figure 2c, indicated by an increase in the oxidative current close to 3.8 V vs. Na^+/Na. A larger gas release of cells with PC electrolyte compared to ethers has been also recently quantified by differential electrochemical mass spectrometry (DEMS).[22] Note that in the early work by Yabuuchi et al., the voltage profiles for P2-FMO appear more defined and the capacity is slightly higher in the early cycles which is likely due to the differences in experimental conditions (voltage window, current density, electrolyte composition).[23]

The cycling stability of P2-FMO in 0.5 M $NaPF_6$/PC and LHCE/G2 is compared in Figure 3c. As apparent from the stability data, the capacity of the 0.5 M $NaPF_6$/PC -based cell quickly drops to 95 mAh g^{-1} within 30 cycles (68% retention), whereas the cell with LHCE/G2 retains a capacity of 115 mAh g^{-1} after 150 cycles. The average Coulomb efficiency over cycling

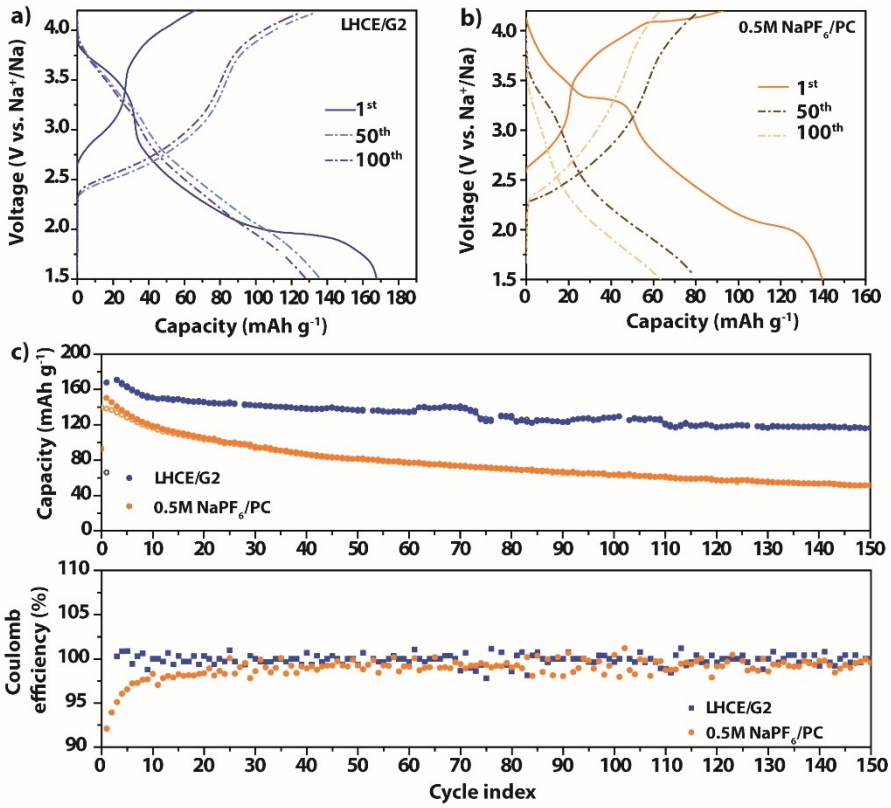

Figure 3. Charge/discharge profiles of P2-$Na_{2/3}Fe_{1/2}Mn_{1/2}O_2$ (P2-FMO) in half-cells at 0.02 A g^{-1} in (a) LHCE/G2 and (b) 0.5 M $NaPF_6$/PC electrolytes; (c) cycling stability and Coulomb efficiency comparison in LHCE/G2 and 0.5 M $NaPF_6$/PC electrolytes in half-cells. (G2 – diglyme, PC – propylene carbonate, LHCE – localized high concentration electrolyte).

Research Article
doi.org/10.1002/batt.202400744
Chemistry Europe
European Chemical Societies Publishing

remains consistent at 99.90 ± 0.44 %. The inferior cycling performance of P2-FMO in other carbonate electrolytes is reported in some of the previous reports. For instance, Ying et al. reported a 38 % capacity retention after 30 cycles (1 M $NaClO_4$/PC with 2 % FEC additive) that can be improved to 75 % by modifying the synthesis step.[24] The low stability is typically attributed to several factors, such as the P2-O2 phase transition at a cut-off voltage above 4 V and the dissolution of Mn^{2+} in the electrolyte upon discharging to 1.5 V. In any case, the transition from carbonate to LHCE/G2 electrolyte did not fully halt the capacity degradation of P2-FMO, which highlights the necessity for additional material-level optimization. However, the observed enhancement in cycling stability underscores the critical significance of employing a suitable electrolyte even during the initial screening of electrode materials in half-cells. It can be noted that the cycling stability test in DE/G2 electrolyte was impossible due to continuous oxidative decomposition close to 4.0 V vs Na^+/Na (Figure S6).

Afterward, the LHCE/G2 electrolyte was utilized to test the cycling stability of another P2-type (P2-NMO) cathode, which is particularly interesting for SIBs owing to its high capacity and moisture-resistant properties.[25] The voltage profiles of P2-NMO in LHCE/G2 (Figure 4a) show several steps related to the Ni and Mn redox and match well with the previous reports.[26] The cell delivers an initial discharge capacity of 170 and 130 mAh g^{-1} (at 0.02 A g^{-1} ≈ 0.1 C) at the 1st and 2nd discharge cycle. Notably, the P2-NMO cathode displayed excellent capacity retention in LHCE/G2, delivering 120 mAh g^{-1} after 300 cycles (Figure 4b). The charge/discharge profiles before and after cycling show overlapping redox plateaus with a negligible shift in the voltage. This cycling performance of P2-NMO surpasses the stability reported in carbonate electrolytes and many substituted materials within this family, as compared in Table S1.

The fact that such a stable cycle life can be achieved is quite surprising, as one would expect a faster fading because of the stepped voltage profile. Steps in the voltage profile indicate phase transitions and it is common sense that they are undesired for obtaining stable cycling. The most prominent strategy to improve the cycle life of layered CAM is therefore doping which can effectively reduce the number of phase transitions.[27] The results, however, show that the LHCE electrolyte can enable stable cycling of layered CAM with a stepped voltage profile. This indicates that the compatibility between the electrode and the electrolyte might be at least equally important.

The compatibility of the LHCE/G2 electrolyte was further tested with an O3-type (O3-NFMO) cathode, as earlier studies on pristine O3-NFMO were carried out in carbonate electrolytes. The layered oxides with the O3 structure typically show a less efficient transport of Na^+ compared to the P2 structure, however, O3-layered CAM have the benefit of containing more Na in their structure, i.e. they provide higher capacity. Like many other oxide cathodes, however, the structural degradation and fast capacity fading of O3-NFMO during cycling is also a concern, which has led the research interest toward stabilizing the pristine material by introducing other substituents to the crystal structure. Although O3-NFMO typically exhibits low cycling stability in carbonate electrolytes during half-cell characterization, this cathode material remains commercially appealing. The current work suggests that the choice of electrolyte for half-cell evaluation may significantly contribute to the observed performance limitations, rather than the

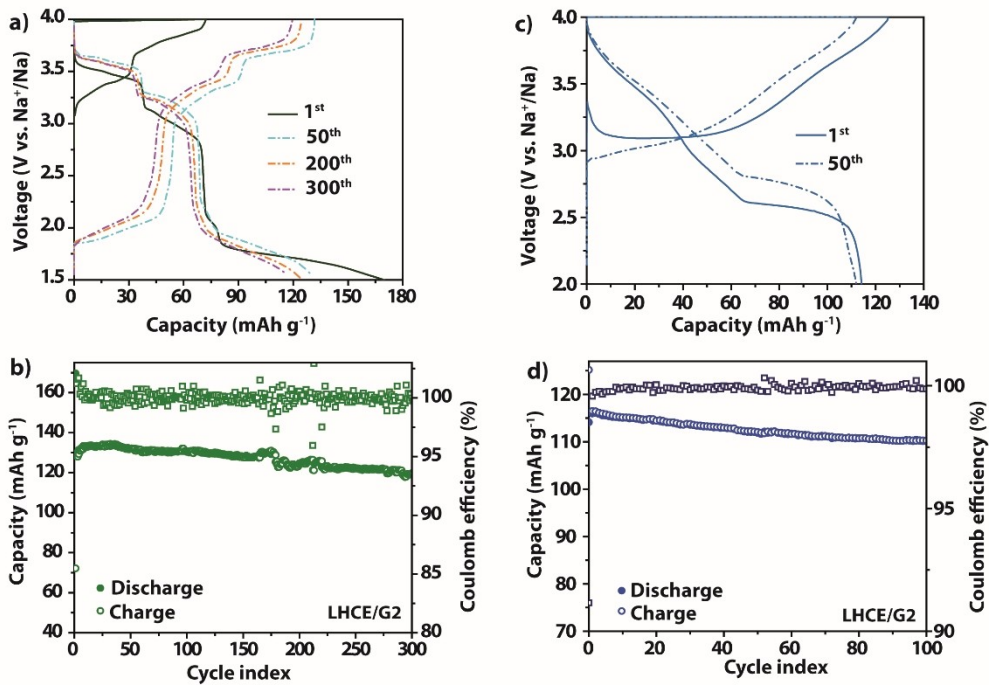

Figure 4. Charge/discharge profiles and cycling stability of (a) – (b) P2-$Na_{2/3}Ni_{1/3}Mn_{2/3}O_2$ (P2-NMO) at 0.02 A g^{-1} and (c) - (d) O3-$NaNi_{1/3}Fe_{1/3}Mn_{1/3}O_2$ (O3-NFMO) cathodes at 0.1 A g^{-1} in LHCE/G2 electrolyte in half-cells (G2 – diglyme, LHCE – localized high concentration electrolyte).

Research Article
doi.org/10.1002/batt.202400744
Chemistry Europe
European Chemical Societies Publishing

inherent instability of the O3-NFMO cathode itself. As shown in Figure 4c, the material delivers 114 mAh g^{-1} capacity 0.1 A g^{-1} and could retain 95% of the initial capacity after 100 cycles (Figure 4d). On the contrary, the cycling performance of the material in the 1 M $NaPF_6$/PC electrolyte shows severe capacity fading resulting in only 57% capacity retention in 50 cycles (Figure S7a and b). This difference in the cycling performance is significant, which further supports the suitability of LHCE/G2 electrolyte over 1 M $NaPF_6$/PC in SIB cells.

The dissolution of transition metals in the liquid carbonate electrolyte is often accounted as the reason for capacity loss during cycling of O3-type cathodes. To verify this factor, the cycled O3-NFMO cells were opened, and the cell components were characterized by SEM and EDX analysis (Figure S8 and S9). The separator recovered from the 1 M $NaPF_6$/PC electrolyte (Figure S8b) shows a significant brown color compared to the LHCE/G2 counterpart (Figure S8a). However, the EDX analysis confirms the absence of transition metals in both separators. The post-cycled cathodes also show a similar relative compositions of Ni, Mn, and Fe, suggesting no or negligible possibility of cathode dissolution in these electrolytes (Figure S9a-c). These observations suggest that the better cycling stability of O3-NFMO in the LHCE/G2 electrolyte is mainly due to its better anodic stability and electrochemical stability than 1 M $NaPF_6$/PC. The cycling stability of the pristine O3-NMFO in LHCE/G2 electrolytes are further compared with some of the modified or substituted materials belonging to this family tested in dilute carbonate electrolytes, as detailed in Table S1.

Conclusions

In conclusion, this study assessed the performance of three commonly studied layered transition metal oxide cathodes for SIBs in the diglyme-based localized high concentration electrolyte (LHCE/G2). Compared to the commonly used dilute electrolytes based on carbonate solvents, LHCE/G2 exhibited superior cycling stability for the cathodes in half-cells with sodium metal counter electrode. Notably, the plating and stripping of sodium in Na/Na symmetric cell using LHCE/G2 displayed a consistently stable voltage profile over 500 hours, indicative of its robust electrochemical stability on sodium metal. In addition, the monoglyme (G1) and triglyme (G3) variants of LHCE also showed favorable plating/stripping behavior and improved oxidation stability, which can be considered as the main factors enabling the improved cycle life. These findings suggest that glyme-based LHCEs could mitigate electrolyte-related degradation, thereby enhancing the long-term cycling stability of SIB materials in half-cell configuration. Given the ease of preparation, the application of LHCEs can also be scaled up and extended to full cell configuration, especially for high-voltage applications. However, the use of highly fluorinated diluents could increase costs, and the electrolyte's lower ionic conductivity may affect its rate performance at low temperature.

Experimental Section

Materials & Methods

Materials

Sodium bis(fluorosulfonyl)imide (NaFSI) and sodium hexafluorophosphate ($NaPF_6$) salts were procured from Solvionic and E-Lyte, respectively. Monoglyme (G1), diglyme (G2), triglyme (G3), propylene carbonate (PC), and N-methylpyrrolidon (NMP) solvents were supplied by Sigma-Aldrich. 1, 1, 2, 2-Tetrafluoroethyl-2, 2, 3, 3-tetrafluoropropyl ether (TTE) was supplied by Apolo Scientific. The solvents were dried by molecular sieve for 2 days before use. The O3-$NaNi_{1/3}Fe_{1/3}Mn_{1/3}O_2$ (O3-NFMO) cathode material was purchased from MTI Corporation. P2-$Na_{2/3}Ni_{1/3}Mn_{2/3}O_2$ (P2-NMO) and P2-$Na_{2/3}Fe_{1/2}Mn_{1/2}O_2$ (P2-FMO) cathodes were synthesized in lab via the sol-gel method and solid-state synthesis method, respectively, following the previous literature. The synthesis methods are described in the supporting information. Sodium metal supplied by BASF was cut into 12 mm disks. Whatman glass fiber separators (GF/A) were dried at 80 °C under vacuum before being used in the cells. The conducting carbon black Super P®Li from Imerys and Kynar polyvinylidene fluoride (PVDF) binder were also dried at 80 °C under vacuum before use.

Electrolyte and Electrode Preparation

All the electrolytes were prepared in an Ar-filled glovebox with O_2 and H_2O levels < 0.1 ppm. For G1 and G2-based LHCEs (LHCE/G1 and LHCE/G2, respectively), the NaFSI salt was first completely dissolved in the solvent followed by adding the TTE diluent. For the G3-based LHCE (LHCE/G3), the salt was dissolved into the mixture of G3 and TTE due to the limited solubility of NaFSI in G3. The mole ratios of NaFSI salt, glyme solvent (G1, G2, or G3), and TTE diluent in LHCE/G1, LHCE/G2, and LHCE/ G3 electrolytes were 1 : 2.25 : 3, 1 : 1.5 : 3, and 1 : 1.12 : 3, respectively. A glyme-based dilute electrolyte, 1 M NaFSI in diglyme (DE/G2), was used for comparison, along with propylene carbonate (PC) solvent-based electrolytes: 1 M $NaPF_6$/PC, 0.5 M $NaPF_6$/PC.

The electrodes were prepared from a homogeneous slurry of the active material, conducting carbon, and PVDF (with 8 : 1 : 1 ratio) in NMP solvent. The slurry was coated onto a carbon-coated Al (C/Al) foil by the doctor-blade method and the dried electrodes were punched into 12 mm diameter disks. The electrodes were finally dried at 120 °C under vacuum and directly transferred into the glove box. The weight of the active material in the electrodes was 1–3 mg cm^{-2}.

Electrochemical Measurement

The temperature-dependent ionic conductivity of the electrolytes was measured using the high-temperature conductivity cell (HTCC) from BioLogic. The electrochemical tests of the different cathodes in SIB half-cell configurations, Na|Na symmetric cells, Na|C/Al cells, etc., were carried out with a Neware battery cycler and BioLogic BCS workstation at room temperature (≈25 °C).

Physical Characterization of Electrolytes and Electrodes

Raman measurements were carried out on a Renishaw inVia Raman microscope coupled to Raman spectrometer with a laser wavelength of 785 nm. The Fourier-transform infrared spectroscopy characterization of the electrolytes was carried out using a Perkin-Elmer ATR-FTIR instrument inside an N_2-filled glovebox. The

morphology and elemental analysis of the electrodes were characterized by a Scanning Electron Microscope (SEM) built with an Energy Dispersive X-ray Spectroscopy (EDX) detector from Thermofisher Scientific.

Supporting Information

The authors have cited additional references within the Supporting Information.[28]

Acknowledgements

M.G. acknowledges the Alexander von Humboldt Foundation (AvH Stiftung, Germany) for research funding for Postdoctoral researchers. The project received funding from the Bundesministerium für Bildung und Forschung (BMBF) over the projects NATTER (03XP0186B) and from the European Research Council (ERC) under the European Union's Horizon 2020 research and innovation programme (grant agreement No. [864698], SEED). Open Access funding enabled and organized by Projekt DEAL.

Conflict of Interests

There are no conflicts to declare.

Data Availability Statement

The data that supports the findings of this study are available from the corresponding author upon reasonable request.

Keywords: Localized high concentration electrolyte (LHCE) · Layered oxide cathodes · Sodium metal anode · Electrochemical stability · Ether electrolytes

[1] a) T. Song, E. Kendrick, *Journal of Physics: Materials* **2021**, *4*, 032004; b) W. Zuo, A. Innocenti, M. Zarrabeitia, D. Bresser, Y. Yang, S. Passerini, *Acc. Chem. Res.* **2023**, *56*, 284–296.
[2] a) Y. Fang, X.-Y. Yu, X. W. Lou, *Angew. Chem. Int. Ed.* **2017**, *56*, 5801–5805; b) J. Alvarado, C. Ma, S. Wang, K. Nguyen, M. Kodur, Y. S. Meng, *ACS Appl. Mater. Interfaces* **2017**, *9*, 26518–26530.
[3] Y. You, A. Manthiram, *Adv. Energy Mater.* **2018**, *8*, 1701785.
[4] K. Pfeifer, S. Arnold, J. Becherer, C. Das, J. Maibach, H. Ehrenberg, S. Dsoke, *ChemSusChem* **2019**, *12*, 3312–3319.
[5] D. I. Iermakova, R. Dugas, M. R. Palacín, A. Ponrouch, *J. Electrochem. Soc.* **2015**, *162*, A7060.
[6] a) R. Rodriguez, K. E. Loeffler, S. S. Nathan, J. K. Sheavly, A. Dolocan, A. Heller, C. B. Mullins, *ACS Energy Lett.* **2017**, *2*, 2051–2057; b) C. Zhu, D. Wu, Z. Wang, H. Wang, J. Liu, K. Guo, Q. Liu, J. Ma, *Adv. Funct. Mater.* **2024**, *34*, 2214195.
[7] a) K. Westman, R. Dugas, P. Jankowski, W. Wieczorek, G. Gachot, M. Morcrette, E. Irisarri, A. Ponrouch, M. R. Palacín, J. M. Tarascon, P. Johansson, *ACS Appl. Energ. Mater.* **2018**, *1*, 2671–2680; b) M. Goktas, C. Bolli, J. Buchheim, E. J. Berg, P. Novák, F. Bonilla, T. Rojo, S. Komaba, K. Kubota, P. Adelhelm, *ACS Appl. Mater. Interfaces* **2019**, *11*, 32844–32855.
[8] Z.-L. Xu, K. Lim, K.-Y. Park, G. Yoon, W. M. Seong, K. Kang, *Adv. Funct. Mater.* **2018**, *28*, 1802099.
[9] a) X. Ren, L. Zou, S. Jiao, D. Mei, M. H. Engelhard, Q. Li, H. Lee, C. Niu, B. D. Adams, C. Wang, J. Liu, J.-G. Zhang, W. Xu, *ACS Energy Lett.* **2019**, *4*, 896–902; b) Y. Yamada, M. Yaegashi, T. Abe, A. Yamada, *Chem. Commun.* **2013**, *49*, 11194–11196.
[10] Y.-S. Hu, Y. Lu, *ACS Energy Lett.* **2020**, *5*, 3633–3636.
[11] J. Chen, H. Zhang, M. Fang, C. Ke, S. Liu, J. Wang, *ACS Energy Lett.* **2023**, *8*, 1723–1734.
[12] X. Cao, H. Jia, W. Xu, J.-G. Zhang, *J. Electrochem. Soc.* **2021**, *168*, 010522.
[13] W. W. A. van Ekeren, M. Albuquerque, G. Ek, R. Mogensen, W. R. Brant, L. T. Costa, D. Brandell, R. Younesi, *J. Mater. Chem. A* **2023**, *11*, 4111–4125.
[14] H. K. Bergstrom, B. D. McCloskey, *ACS Energy Lett.* **2024**, *9*, 373–380.
[15] a) I. Hasa, S. Passerini, J. Hassoun, *J. Power Sources* **2016**, *303*, 203–207; b) M. P. Do, N. Bucher, A. Nagasubramanian, I. Markovits, T. Bingbing, P. J. Fischer, K. P. Loh, F. E. Kühn, M. Srinivasan, *ACS Appl. Mater. Interfaces* **2019**, *11*, 23972–23981.
[16] a) L. O. S. Colbin, C. A. Hall, A. S. Etman, A. Buckel, L. Nyholm, R. Younesi, *Energy Advances* **2024**, *3*, 143–148; b) L. Otaegui, E. Goikolea, F. Aguesse, M. Armand, T. Rojo, G. Singh, *J. Power Sources* **2015**, *297*, 168–173.
[17] a) Y. Chen, F. Huang, M. Xie, Y. Han, W. Li, Y. Jie, X. Zhu, T. Cheng, R. Cao, S. Jiao, *ACS Appl. Mater. Interfaces* **2024**, *16*, 47581–47589; b) X. Chen, Y. Meng, D. Xiao, Y. Wu, L. Qin, *Energy Storage Mater.* **2023**, *61*, 102923.
[18] A. Mathew, M. J. Lacey, D. Brandell, *Journal of Power Sources Advances* **2021**, *11*, 100071.
[19] C. Zor, S. J. Turrell, M. S. Uyanik, S. Afyon, *Advanced Energy and Sustainability Research* **2024**, *5*, 2300001.
[20] a) A. C. S. Jensen, H. Au, S. Gärtner, M.-M. Titirici, A. J. Drew, *Batteries & Supercaps* **2020**, *3*, 1306–1310; b) S. Tsuzuki, W. Shinoda, S. Seki, Y. Umebayashi, K. Yoshida, K. Dokko, M. Watanabe, *ChemPhysChem* **2013**, *14*, 1993–2001.
[21] L. F. Pfeiffer, Y. Li, M. Mundszinger, J. Geisler, C. Pfeifer, D. Mikhailova, A. Omar, V. Baran, J. Biskupek, U. Kaiser, P. Adelhelm, M. Wohlfahrt-Mehrens, S. Passerini, P. Axmann, *Chem. Mater.* **2023**, *35*, 8065–8080.
[22] J. Geisler, L. Pfeiffer, G. A. Ferrero, P. Axmann, P. Adelhelm, *Batteries & Supercaps* **2024**, *7*, e202400006.
[23] N. Yabuuchi, M. Kajiyama, J. Iwatate, H. Nishikawa, S. Hitomi, R. Okuyama, R. Usui, Y. Yamada, S. Komaba, *Nat. Mater.* **2012**, *11*, 512–517.
[24] Y. Bai, L. Zhao, C. Wu, H. Li, Y. Li, F. Wu, *ACS Appl. Mater. Interfaces* **2016**, *8*, 2857–2865.
[25] a) J. Zhang, W. Wang, W. Wang, S. Wang, B. Li, *ACS Appl. Mater. Interfaces* **2019**, *11*, 22051–22066; b) Z. Lu, J. R. Dahn, *Chem. Mater.* **2001**, *13*, 1252–1257.
[26] Q. Liu, Z. Hu, M. Chen, C. Zou, H. Jin, S. Wang, Q. Gu, S. Chou, *J. Mater. Chem. A* **2019**, *7*, 9215–9221.
[27] Y. Xiao, N. M. Abbasi, Y.-F. Zhu, S. Li, S.-J. Tan, W. Ling, L. Peng, T. Yang, L. Wang, X.-D. Guo, Y.-X. Yin, H. Zhang, Y.-G. Guo, *Adv. Funct. Mater.* **2020**, *30*, 2001334.
[28] a) L. Yang, L.-Y. Kuo, J. M. López del Amo, P. K. Nayak, K. A. Mazzio, S. Maletti, D. Mikhailova, L. Giebeler, P. Kaghazchi, T. Rojo, P. Adelhelm, *Adv. Funct. Mater.* **2021**, *31*, 2102939; b) G. Singh, B. Acebedo, M. C. Cabanas, D. Shanmukaraj, M. Armand, T. Rojo, *Electrochem. Commun.* **2013**, *37*, 61–63; c) K. Park, D. Han, H. Kim, W.-s. Chang, B. Choi, B. Anass, S. Lee, *RSC Adv.* **2014**, *4*, 22798–22802; d) J. Xu, S.-L. Chou, J.-L. Wang, H.-K. Liu, S.-X. Dou, *ChemElectroChem* **2014**, *1*, 371–374; e) S. Altin, A. Bayri, E. Altin, E. Oz, S. Yasar, S. Altundağ, M. Harfouche, S. Avci, *Energy Technol.* **2021**, *9*, 2001130; f) H. Wang, B. Yang, X.-Z. Liao, J. Xu, D. Yang, Y.-S. He, Z.-F. Ma, *Electrochim. Acta* **2013**, *113*, 200–204; g) H. Wang, X.-Z. Liao, Y. Yang, X. Yan, Y.-S. He, Z.-F. Ma, *J. Electrochem. Soc.* **2016**, *163*, A565; h) L. Sun, Y. Xie, X.-Z. Liao, H. Wang, G. Tan, Z. Chen, Y. Ren, J. Gim, W. Tang, Y.-S. He, K. Amine, Z.-F. Ma, *Small* **2018**, *14*, 1704523.

Manuscript received: November 24, 2024
Revised manuscript received: March 11, 2025
Version of record online: March 24, 2025